# Supporting Information

## Kuga et al. 10.1073/pnas.1502796112

### SI Materials and Methods

**The Nebulotron Plasma Experiment.** The Nebulotron experiment (Fig. S1) consists of a vacuum glass line and a quartz reactor where a high-frequency discharge (2.45 GHz) is generated by a microwave generator (MPG 4–470 model; Opthos Instruments). A microwave cavity [a modified McCaroll type (1)] is used to increase the electric field in the gas flowing in the quartz reactor, and is cooled down with compressed air. Gas mixtures of CO only or CO + $N_2$, with or without the addition of noble gases, are flowed continuously through the plasma discharge at a pressure of ∼1 mbar. Notably, two noble gas tanks were used during the experiments, containing Ne, Ar, Kr, Xe mixed with $N_2$ or He, respectively (hereafter M1 and M2; e.g., Fig. S1). Flow rates of gas mixtures are controlled with two mass flow controllers (Brooks Delta Smart II, calibrated on CO), of 50 sccm and 10 sccm, respectively. Typical experiments were run with a gas flow of 6–10 sccm, for 2–6 h (Tables S1 and S2). Electrons and heavy particles at ∼800–1,000 K (2, 3) initiate dissociation and ionization of molecular and atomic species. Resulting chemical reactions form hydrocarbons and N-bearing molecules and eventually lead to the polymerization of monomers and to the growth of solid particles. In the Nebulotron, solid compounds are likely formed at temperatures of <700 K as the dust and the gas are out of equilibrium (2). The organic aerosols grow up on the quartz tube surfaces and are recovered by gently scratching the surfaces. The synthetic solids are brown to dark in color. They consist of 1- to 100-μm aggregates with elongated shapes and are mostly insoluble. Averaged solid production rates are in the range 4–11 mg/h, depending on the experimental conditions (starting gas mixture composition, duration, electric power of the discharge). We calculated the carbon gas-to-solid yields during each experiment [percent of carbon in the flowing gas mixture (e.g., CO) that was converted into solid organic carbon] (Table S2) to evaluate the efficiency of carbon incorporation into the synthesized solids. They should be considered as minimum values because the synthesized samples could only be partially recovered by scratching the glass walls of the reaction zone. An estimate of the plasma parameters (neutral and electronic temperatures, electron density, etc.) of the Nebulotron plasma can be found in ref. 3.

**Analytical Techniques.**

***Elemental analysis.*** C, H, N, and O elemental analyses were carried out at the Service d'Analyses Elémentaires (Université de Lorraine). Bulk C, N, and H elemental composition were determined on the same aliquots (typically 1 mg loaded into tin capsules). Combustion analyses at 940 °C in a quartz oxidation column were conducted using a Thermo Finnigan Flash EA 1112 series CHN analyzer. Bulk O elemental composition was determined on a separate aliquot, by pyrolysis at 1,060 °C on a quartz reactor. The measurement precision for elemental abundances is typically of the order 1–3% of the reported values (Table S1).

***Infrared spectroscopy.*** IR measurements were performed with a Brucker Hyperion 3000 infrared spectrometer coupled to a microscope, with a 4 $cm^{-1}$ spectral resolution from 4,000 $cm^{-1}$ to 600 $cm^{-1}$ (Institut de Planétologie et d'Astrophysique de Grenoble). Organic grains recovered from the Nebulotron reactor were deposited on a diamond window (3.0 × 0.5 mm) and crushed by applying a second diamond window to get a thin sample layer and a roughly identical thickness from one sample to another (see ref. 4 for detailed procedure). The thickness was visually controlled with the microscope focus. Five to ten spectra were acquired on each sample. Complementary measurements were acquired under vacuum at 80 °C in an environmental cell to control the water removal from sample surfaces. This was done for Neb-CO28 sample (Table S1) only (Neb-CO28# in Fig. 1). A baseline spline fit was used to correct IR spectra. Baseline-corrected spectra were normalized to the 1,600 $cm^{-1}$ absorbance.

***Raman spectroscopy.*** Raman spectra were collected at 514-nm and 244-nm wavelengths. Raman measurements with a 514-nm excitation wavelength were performed with a LabRam Raman spectrometer (Horiba Jobin-Yvon) equipped with a 600 g/mm grating (GéoRessources Laboratory). The laser beam was focused through an 80× objective, leading to a ∼1-μm circular spot. Typical power on the sample and acquisition time were 4 μW and 200 s, respectively. Only Nebulotron organics containing low amounts of nitrogen (i.e., Neb-CO– and Neb-COGR–type samples; Table S1) could be analyzed at this excitation wavelength (Fig. S2); the samples with a high nitrogen content showed a too strong fluorescence background. The fluorescence background of the 514-nm spectra was corrected by subtracting a linear baseline, and spectra were normalized to the peak intensity of the G band. Raman spectral parameters of the first-order carbon bands such as width at half maximum (FWHM-D, FWHM-G), peak position ($\omega_D$, $\omega_G$), and ratio of peak intensity of the D and G bands ($I_D/I_G$) were obtained by applying a Lorentzian Breit–Wigner–Fano (LBWF) fit (see refs. 4 and 5 for detailed procedure).

UV Raman spectra were obtained with a Horiba Jobin-Yvon LabRam system with a frequency-doubled $Ar^+$ laser delivering a 244-nm wavelength (Laboratoire de Géologie, Ecole Normale Supérieure). A 600 g/mm grating and a 40× objective were used, leading to a spot diameter of ∼5 μm. The laser power delivered to the sample was limited to 300 μW in this configuration. Spectra were acquired in the 500–4,000 $cm^{-1}$ spectral range. Raw 244-nm spectra are devoid of background fluorescence (Fig. S3), and were reduced along the same procedure applied to the 514-nm spectra, and fitted with an LBWF model.

***Transmission electron microscopy.*** Transmission electron microscopy (TEM) images of Nebulotron organics were acquired on a Philips CM20 and a JEOL ARM 200F operating at 200 kV (Institut Jean l'Amour, Université de Lorraine). The Nebulotron dust grains were dispersed in ethanol on TEM grids covered by amorphous carbon films. The structural organization was directly imaged by using the "high-resolution mode" (350,000× magnification).

***Noble gas mass spectrometry.*** The noble gases (Ar, Kr, and Xe) trapped in the samples synthesized in the Nebulotron setup were extracted by heating the samples in a double-walled quartz furnace at Centre de Recherches Pétrographiques et Géochimiques (6). Before introduction into the furnace, a fraction of the Nebulotron samples was weighted (50 μg to 1 mg) on a precise weighing scale and wrapped in platinum foils or in nickel crucibles, previously degassed at 800 °C under ultravacuum. A horizontal quartz tube, heated by a classical furnace (25 °C < $T$ < 900 °C), was associated with a vertical induction furnace also made of quartz (T > 900 °C). Once the samples were introduced into the furnace, the system was baked at ∼100 °C at high vacuum ($10^{-9}$ mbar). The Nebulotron samples were heated in a first step at 200 °C to check air contamination and in a second step at 1,400 °C to completely degrade the carbon structure. A second heating step at 1,450 °C was systematically performed to ensure the total extraction of the gases. The temperature of the horizontal quartz furnace was monitored with an accuracy of ∼50 °C using a thermocouple located outside the tube. To calibrate the temperature of the induction furnace, we used an optical pyrometer with a precision

of ±100 °C. Each heating step lasted 20 min to 30 min. The released gas was purified using two Ti–Zr getters to remove active gases (10 min at 800 °C, 10 min at room temperature). Ar was separated from Kr and Xe using a cold finger plunged in liquid nitrogen and was analyzed first. The Kr–Xe fraction was analyzed in a second step. Analysis of noble gases was performed with a sector-type mass spectrometer. Each sample has been bracketed by two standards for which the amounts of noble gases were adjusted to be comparable to the sample abundance. Blank contributions are variable for each heavy noble gas: <1% for xenon, <20% for Kr, and ~90% for Ar. No specific blank correction was applied for Xe, while Kr concentrations and isotopic ratios were blank corrected. Considering Ar, we used the blank contribution ($2.1 \times 10^{-13}$ moles of $^{40}$Ar) for computing an upper limit of the Ar content of the Nebulotron solids as well as the elemental fractionation factor (e.g., Fig. 4). A trapping yield (gas to solid) for Xe was calculated (Table S2) using the Xe content in the solids and the amount of Xe (gas) that flowed during the experiment. He and Ne contents in the Nebulotron organics could not be measured because of their low amounts in the synthesized samples.

**Comparison of Laboratory Synthesized Organics with Refractory Organic Solids from Primitive Chondrites.** The elemental analyses and FTIR data show that the N-poor Nebulotron samples (produced from CO + traces of $H_2/H_2O$ ± noble gases) display a chemical composition close to that of IOM from unheated chondrites (Tables S1 and S2 and Fig. 1*A*). N-poor Nebulotron samples display elemental ratios in the range of those of IOM from primitive chondrites (7) and their FTIR spectra are comparable to those of IOM. The N-poor Nebulotron samples are O-rich and aliphatic-poor compared with chondritic IOM as shown by FTIR spectra (Fig. 1*A*).

Raman and HRTEM studies also support common structural features between the Nebulotron-synthesized organics and IOM or other extraterrestrial organics (Figs. 2 and 3). Both the carbon nanotextures (Fig. 2) and the Raman spectral parameters (Fig. 3) are comparable [although not exactly identical, as illustrated by the D-band parameters (Fig. 3*A*)]. Interestingly, the Nebulotron samples plot close to the extraterrestrial primitive organics in the Raman spectral parameters space (Fig. 3). Altogether, these observations show that organosynthesis from very simple gas molecules at temperatures of >500 K can account for the production of complex and unsaturated organic compounds with carbon structural disorder fairly similar to that of chondritic IOMs.

The elemental and isotopic fractionations of trapped Xe-Q and Kr-Q in meteorites relative to the solar composition (8) are well reproduced in the Nebulotron plasma experiment (Fig. 4). Ionization, which increases dramatically the trapping efficiency of noble gases in growing solids (9), may also account for the extremely high noble gas content of Phase Q (8).

FTIR and 244-nm Raman spectra show that organics produced in the Nebulotron setup from a mixture of $CO+N_2$ (plus traces of H) are richer in nitrogen (up to 22% mol) than chondritic IOM (max. 4% mol in CR-type chondrites; see refs. 7, 10, 11). This difference was already observed for laboratory analogs produced in a $N_2$–$CH_4$ plasma [tholins from the PAMPRE setup (12)] (Fig. 1 and Fig. S3). Interestingly, N-rich refractory organics have been identified in some IDPs (13) and in UCAMMs (14), which are believed to be of cometary origin. Both N-rich Nebulotron samples and PAMPRE tholins display fairly similar FTIR spectra to that of UCAMM (but with either too much oxygen or aliphatic abundance; Fig. 1).

The low nitrogen abundance in chondritic IOM may result from different processes. Organic precursors of IOM might have been initially N-rich, such as "cometary" organics. Processing in the disk or onto the parent body might have resulted in selective loss of nitrogen (12). The fact that IOM still contains trapped noble gases with a common composition among different classes of meteorites may not support this possibility. However, one could argue that Phase Q is only a small and refractory fraction of IOM, so that nitrogen would have been lost from more labile sites than Phase Q. Alternatively, meteoritic IOM might have originated from synthesis of organics in a gas of noncanonical composition, that is, in a gaseous environment depleted in nitrogen relative to C-bearing species, or from precursors having trapped preferentially C and H relative to N. Both scenarios have to be investigated in detail.


1. McCarroll B (1970) An improved microwave discharge cavity for 2450 MHz. *Rev Sci Instrum* 41:279.
2. Fridman A (2008) *Plama Chemistry* (Cambridge Univ Press, New York).
3. Kuga M, et al. (2014) Nitrogen isotopic fractionation during abiotic synthesis of organic solid particles. *Earth Planet Sci Lett* 393:2–13.
4. Quirico E, et al. (2014) Origin of insoluble organic matter in type 1 and 2 chondrites: New clues, new questions. *Geochim Cosmochim Acta* 136:80–99.
5. Bonal L, Quirico E, Bourot-Denise M, Montagnac G (2006) Determination of the petrologic type of CV3 chondrites by Raman spectroscopy of included organic matter. *Geochim Cosmochim Acta* 70(7):1849–1863.
6. Marrocchi Y, Derenne S, Marty B, Robert F (2005) Interlayer trapping of noble gases in insoluble organic matter of primitive meteorites. *Earth Planet Sci Lett* 236(3-4):569–578.
7. Alexander CMOD, Fogel M, Yabuta H, Cody GD (2007) The origin and evolution of chondrites recorded in the elemental and isotopic compositions of their macromolecular organic matter. *Geochim Cosmochim Acta* 71(17):4380–4403.
8. Busemann H, Baur H, Wieler R (2000) Primordial noble gases in "phase Q" in carbonaceous and ordinary chondrites studied by closed system etching. *Meteorit Planet Sci* 35(5):949–973.
9. Marrocchi, et al. (2011) Adsorption of xenon ions onto defects in organic surfaces: Implications for the origin and the nature of organics in primitive meteorites. *Geochim Cosmochim Acta* 75(20):6255–6266.
10. Orthous-Daunay FR, et al. (2013) Mid-infrared study of the molecular structure variability of insoluble organic matter from primitive chondrites. *Icarus* 223(1):534-543.
11. Dobrica E, Engrand C, Quirico E, Montagnac G, Duprat J (2011) Raman characterization of carbonaceous matter in CONCORDIA Antarctic micrometeorites. *Meteorit Planet Sci* 46(9):1363–1375.
12. Bonnet J-Y, et al. (2015) Formation of analogs of cometary nitrogen-rich refractory organics from thermal degradation of tholin and HCN polymer. *Icarus* 250:53–63.
13. Aleon J, Robert F, Chaussidon M, Marty B (2003) Nitrogen isotopic composition of macromolecular organic matter in interplanetary dust particles. *Geochim Cosmochim Acta* 67(19):3773–3783.
14. Dartois E, et al. (2013) UltraCarbonaceous Antarctic micrometeorites, probing the Solar System beyond the nitrogen snow-line. *Icarus* 224(1):243–252.

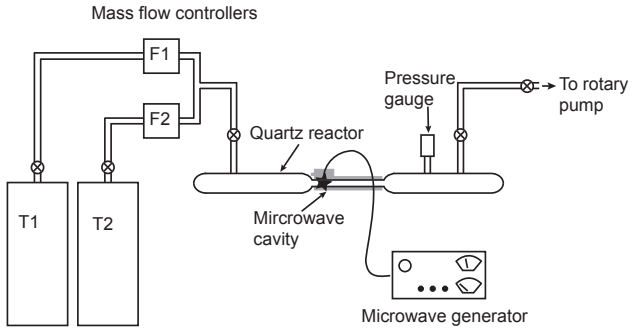


T1 = pure CO

T2 = - pure $N_2$ or,
- M1: $N_2$ (50%), Ne (20%), Ar (10%), Kr (10%), Xe (10%) or,
- M2: He (75%), Ne (15%), Ar (5%), Kr (3%), Xe (2%)

**Fig. S1.** The Nebulotron experimental setup.

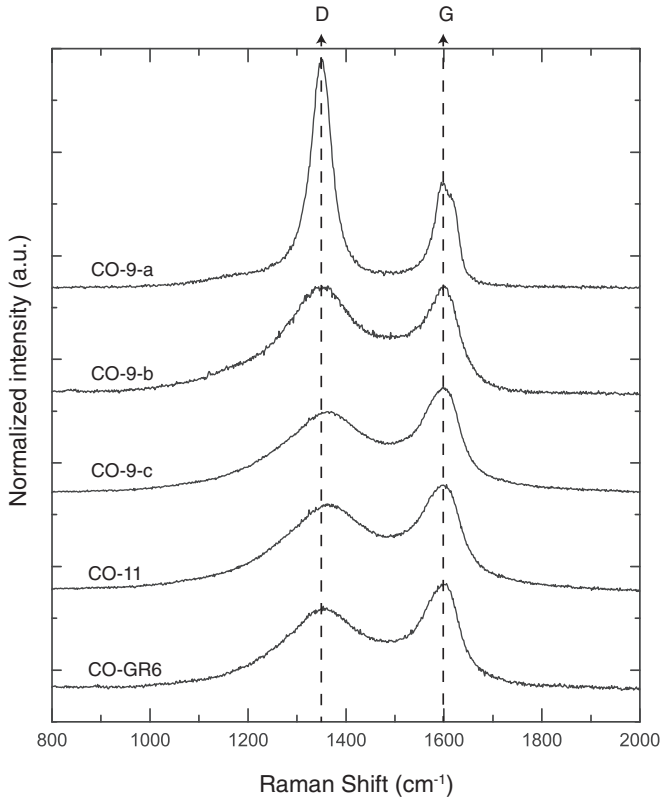


**Fig. S2.** The 514-nm Raman spectra for the N-poor Nebulotron samples. The baseline is subtracted, and the intensity is normalized to the intensity of the G band. The Nebulotron sample CO-9 shows heterogeneity.

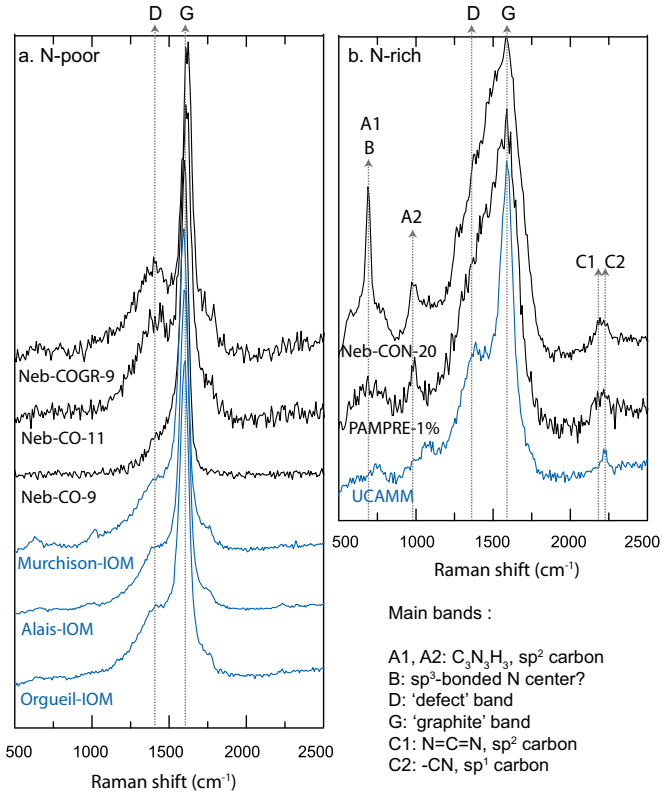


**Fig. S3.** UV 244-nm Raman spectra collected on Nebulotron synthesized solids from CO ± $N_2$ ± noble gases. Spectra of IOMs of unheated chondrites (1), fragment of the UCAMM particle DC119 (2) and tholins from the PAMPRE setup [synthesized from a gas mixture of 1% $CH_4$ in $N_2$, (3)] are shown for comparison. All spectra are normalized to the G band. (*A*) Nitrogen-poor organics. Qualitative observations of the 244-nm Raman spectra show structural heterogeneity among the N-poor Nebulotron samples (from CO or CO–noble gases mixtures). The sample Neb-CO-9 displays a narrow G band and an almost absent D band, clearly reflecting a higher degree of structural organization as shown by HRTEM images (Fig. 2). (*B*) Nitrogen-rich organics. Nebulotron solids produced from a CO–$N_2$ gas mixture display drastically different 244-nm Raman spectra, with (*i*) a larger G band and (*ii*) the appearance of resonant features related to the presence of large amounts of nitrogen in these compounds (2, 4, 5).


1. Quirico E, et al. (2014) Origin of insoluble organic matter in type 1 and 2 chondrites: New clues, new questions. *Geochim Cosmochim Acta* 136:80–99.
2. Dobrica E, Engrand C, Quirico E, Montagnac G, Duprat J (2011) Raman characterization of carbonaceous matter in CONCORDIA Antarctic micrometeorites. *Meteorit Planet Sci* 46(9):1363–1375.
3. Sciamma-O'Brien E, Carrasco N, Szopa C, Buch A, Cernogora G (2010) Titan's atmosphere: An optimal gas mixture for aerosol production? *Icarus* 209(2):704–714.
4. Quirico E, et al. (2008) New experimental constraints on the composition and structure of tholins. *Icarus* 198(1):218–231.
5. Ferrari AC, Rodil SE, Robertson J (2003) Interpretation of infrared and Raman spectra of amorphous carbon nitrides. *Phys Rev B* 67:155306.


**Table S1. Experimental conditions for the production of the Nebulotron organic solids**

| Gas mixture | Percent CO in the gas | N/C gas | He/C gas | Ar/C gas | Xe/C gas | Sample | Duration, min | Total flow rate, sccm | Electric discharge power, W |
|---|---|---|---|---|---|---|---|---|---|
| CO only | 100 | — | — | — | — | CO-9 | 240 | 5 | 60 |
| | | | | | | CO-11 | 240 | 5 | 40 |
| | | | | | | CO28 | 120 | 10 | 30 |
| CO–noble gases (M2) | 83 | — | $1.5 \times 10^{-1}$ | $1.0 \times 10^{-2}$ | $4.0 \times 10^{-3}$ | CO-GR6N | 210 | 6 | 40 |
| | | | | | | CO-GR9 | 120 | 6 | 70 |
| | | | | | | CO-GR29 | 360 | 6 | 30 |
| | | | | | | CO-GR30 | 360 | 6 | 60 |
| CO–$N_2$–noble gases (M1) | 50 | 0.2 | — | $2.0 \times 10^{-2}$ | $2.0 \times 10^{-2}$ | CO-*N*-GR34 | 360 | 6 | 30 |
| CO–$N_2$ | 50 | 0.4 | — | — | — | CO-N2 20N | 360 | 6 | 40 |
| Solar nebula (1) | | 0.25 | 316 | $9.3 \times 10^{-3}$ | $6.5 \times 10^{-7}$ | | | | |


1. Asplund M, Grevesse N, Sauval AJ, Scott P (2009) The chemical composition of the Sun. *Annu Rev Astron Astrophys,* 47:481–522.

**Table S2. Experimental yields (C, Xe), elemental ratios, and Xe content of the Nebulotron samples**

| Gas mixture | Sample | Solid production rate, mg/h | Carbon gas-to-solid yield, % | N/C | H/C | O/C | $^{132}$Xe, × $10^{-12}$ mol/g | $^{132}$Xe trapping yield |
|---|---|---|---|---|---|---|---|---|
| CO only | CO-9 | 3.2 | 2.6 | 0.04 | 0.34 | 0.08 | — | — |
| | CO-11 | 3.2 | 2.1 | 0.08 | 0.49 | 0.27 | — | — |
| | CO28 | — | — | 0.01 | 0.65 | 0.34 | — | — |
| CO-Noble Gases (M2) | CO-GR6N | 2.1 | 0.9 | 0.06 | 0.71 | 0.25 | 6.8 | $1.1 \times 10^{-9}$ |
| | CO-GR9 | 3.8 | 1.6 | 0.06 | 0.56 | 0.22 | 53.7 | $1.4 \times 10^{-8}$ |
| | CO-GR29 | 4.2 | 1.8 | 0.01 | 0.61 | 0.24 | 108 | $3.1 \times 10^{-8}$ |
| | CO-GR30 | 4.2 | 2.1 | 0.02 | 0.46 | 0.14 | 2,390 | $7.0 \times 10^{-7}$ |
| CO-$N_2$-Noble Gases (M1) | CO-N-GR34 | 12 | 3 | 0.5 | 0.9 | 0.6 | 13.4 | $2.2 \times 10^{-9}$ |
| CO-$N_2$ | CO-N2 20N | 3.8 | 1.5 | 0.75 | 0.97 | 0.63 | — | — |